Powdered Ca-activated zeolite for phosphate removal from treated wastewater

M. Hermassi[a,b] , C. Valderrama[a,*], N. Moreno[c], O. Font[c], X. Querol[c], N.H. Batis[b] and J.L. Cortina[a]

[a] Chemical Engineering Department. Universitat Politècnica de Catalunya-Barcelona TECH (Spain)

[b] Department of Biological and Chemical Engineering, National Institute of Applied Sciences and Technology (INSAT), (Tunisia)

[c] Institute of Environmental Assessment and Water Research IDAEA, Consejo Superior de Investigaciones Científicas (CSIC) Barcelona

*Correspondence should be addressed to: César Valderrama

Departament d'Enginyeria Química, Universitat Politècnica de Catalunya

Av. Diagonal 647, 08028, Barcelona Spain

Tel.: 93 4011818, Fax.: 93 401 58 14

Email: cesar.alberto.valderrama@upc.edu

Abstract

BACKGROUND: A powdered zeolitic material synthesised from fly ash (FA) (NaP1-FA) and its Calcium modified form (CaP1-NA) were studied as sorbent materials for the recovery of phosphate from treated wastewater effluents. Phosphate-sorption equilibrium experiments were performed by varying the experimental conditions, including the solution pH, phosphate concentration, and the presence of competing ions.

RESULTS: The maximum phosphate-sorption capacities were 57±5 and 203±11 mgP-PO_4/g for NaP1-FA and CaP1-NA, respectively. The sorption capacities of both zeolites in the pH range expected for wastewater effluents (pH from 7 to 9) were slightly dependent on pH, exhibiting maxima at pH 8. Phosphate removal proceeds through two main mechanisms: a) surface

complexation with ≅AlOH and ≅FeOH groups of the zeolitic structure or unreacted minerals from the FA, and b) the formation of Ca-phosphate phases, mainly brushite.

CONCLUSIONS: The removal mechanisms were confirmed by XRD analyses and P speciation. The stabilities of the phosphate-loaded zeolite samples evaluated by the extraction experiments confirmed their potential availabilities in soil applications. Finally, the higher solubility of brushite compared with that of Hap makes this zeolitic material promising as a novel inorganic zeolite/CaP1-NA/brushite fertiliser.

Keywords: phosphate recovery; powder synthetic zeolite; calcium modification; waste valorisation; brushite; fertilizer

1. Introduction

Increasing energy demands worldwide have led to increased utilisation of coal and the production of large quantities of fly ash (FA) as a waste product. The global production of FA in 2010 exceeded 750 million tons/year, with 38 million tons produced in Europe alone.[1,2] FA is enriched with SiO_2 and Al_2O_3, and thus, it can be transformed by chemical treatment into zeolite-like crystalline materials. The synthesis of zeolites is attracting attention as an effective use for coal fly ash CFA, possibly because of its similar composition to the volcanic material that serves as the precursor of natural zeolites.

Zeolites are microporous aluminosilicate minerals that could be used as ion exchangers in domestic and industrial water purification and softening applications [3]. The substitution of silicon (Si) by aluminium (Al) atoms in the crystal framework leads to extra negative charges that must be balanced by surrounding counter ions (such as Na^+, K^+, Ca^{2+}, and Mg^{2+}); these counter ions can be easily exchanged for other surrounding cations in contact with aqueous solutions. Therefore, several studies on the use of zeolites for the removal of hazardous cations [4,5] and

anions and organic compounds with modified zeolites [6] have been reported. By applying several synthesis methods, different families of zeolites have been synthesised from FA; [6–8] however, few have been successfully converted into pure-phase zeolites.[9,10]

The removal of phosphate from wastewaters has been linked to the need for their reuse and valorisation, both of which could be achieved using a reactive material capable of achieving high phosphate-removal ratios in solution and suitable for use as a fertiliser in soil and agricultural applications.[11] This process could be developed if low-cost sorbents are available.[12] Querol et al.[13] demonstrated the economic and technical viability of synthesising NaP1-FA under mild hydrothermal conditions without using templates. NaP1-FA was evaluated for the removal of toxic metals from acid mine drainage and brines[14] because of its unique ion-exchange and water-sorption properties, which are attributable to its high porosity, surface area, and cation exchange capacity (CEC) and its unusual framework flexibility.[15] NaP1-FA also has a high capacity to adsorb ammonium and potassium K, and it has been evaluated as a slow-release fertiliser; however, the sorption of oxyanions as phosphate is not favoured by the zeolite structure.[16] The use of mixtures of synthetic apatites and natural zeolites as solid media for growing plants and as a fertiliser has been postulated.[17,18] However, because of the low solubility and availability of P from hydroxyapatite (Hap) in soils, efforts have been directed towards the preparation of relatively soluble Hap ($Ca_{10}(PO_4)_6(OH)_2$) and brushite ($CaHPO_4.2H_2O$) by growing crystals on the surface of Ca-containing minerals. These materials include Ca silicates, such as wollasonite;[19] Ca-Al layered double hydroxide; and Hap.[20,21] However, little work has been done to prepare a reactive material to a) efficiently remove phosphate from wastewater effluents in the form of relatively soluble phosphates (e.g., brushite ($\log K_{so}$=6.59))[22] compared to Hap ($Ca_5(PO_4)_3OH$(s), $\log K_{so}$=116.8)[23] and b) to achieve suitable properties for use as a synthetic fertiliser.

In this study, both the Na^+-zeolite (NaP1-FA), synthesised from coal fly ash (CFA), and its Ca-modified form (CaP1-NA) were evaluated as sorbents for phosphate recovery from aqueous

solution. The phosphate-sorption performance was studied by varying the experimental conditions, such as the solution pH, coexisting ions, and initial phosphate concentration. The results are presented in terms of equilibrium isotherms in non-competitive and competitive experiments with other common anions present in wastewater effluents. Furthermore, the phosphate-sorption removal mechanisms were evaluated using a speciation methodology. Finally, the stability of the phosphate-loaded zeolite samples was evaluated by extraction experiments using bicarbonate solutions to determine their potential availability in soil applications.

2. Materials and methods

2.1. Synthesis of NaP1-FA and CaP1-NA

Na^+-zeolite (NaP1-FA) was synthesised from Narcea CFA with 3 mol/L NaOH at 125°C for 8 h using a hydrothermal method, as described elsewhere [13]. Ca-zeolite (Ca^{2+}-zeolite CaP1-NA) was prepared by a cation-exchange process. First, 250 g of NaP1-FA was immersed in 1000 mL of a 0.5-mol/L $CaCl_2$ solution for 1 h at room temperature, which was then filtered through a 0.2-µm membrane filter and rinsed with distilled water to remove the $CaCl_2$ solution [16]. The cation-exchange and washing cycle was repeated five times. The sample obtained was dried for 72 h at 50–60°C.

2.2. Phosphate-removal equilibrium experiments

Phosphate test solutions were prepared by dissolving a weighed amount of $Na_2HPO_4.2H_2O$ in water obtained from a Milli-Q-Academic-A10 apparatus (Millipore Co. France). Batch experiments were performed at room temperature (21±1ºC). Samples of zeolites (0.2 g) were mechanically mixed in special polyethylene stoppered tubes with an aqueous phosphate solution (12 mL) at different initial concentrations of phosphate (100–16,000 mg L-1) until equilibrium was achieved

(24 h). The influence of pH on the phosphate sorption was evaluated by using 0.1-mol/L HCl or NaOH solution to adjust the initial pH. After phase separation with a 0.2-μm syringe filter, the equilibrium pH was measured using a pH electrode (Crison GLP22), and the total phosphate concentration was measured using spectrophotometric colourimetry [24]. The phosphate equilibrium sorption capacity determined using Eq. 1.

$$q_e = (C_0 - C_e)\frac{v}{m_s} \quad (1)$$

where C_0 (mg/L) and C_e (mg/L) represent the initial and equilibrium total phosphate concentrations, respectively; v (L) is the aqueous solution volume; and m_s (g) is the mass of zeolite.

2.3. Phosphate-removal equilibrium experiments in the presence of competing ions

The effect of common coexisting ions in wastewater, such as chloride, sulfate, nitrate, and bicarbonate, on the sorption of phosphate was investigated by adding 300 mg HCO_3^-/L, 300 mg Cl^-/L, 250 SO_4^{2-}/L, and 50 mg NO_3^-/L to 100-15,000 mg P-PO_4^{3-}/L. A given mass of CaP1-NA (0.2 g) was added, and the solution was agitated at 400 rpm for 24 h at 21±2°C. After filtration with a 0.2-μm membrane filter, the residual phosphate concentration was analysed using spectrophotometric colourimetry. The typical values of the effluent streams from secondary treatment at the El Prat wastewater treatment plant (WWTP) (Barcelona, Spain) were used to determine the feed composition.

2.4. Speciation of phosphate-loaded zeolite samples using a sequential extraction protocol

The speciation of phosphorus (P) adsorbed in loaded zeolites (NaP1-FA and CaP1-NA) was achieved using a modified four-step sequential extraction [25–27]. First, 30-mL aliquots of 1000 mg P-PO_4^{3-}/L at pH 7 were equilibrated with pre-weighed tubes containing 3 g of each type of zeolite:

NaP1-FA and CaP1-NA. After shaking for 24 h at room temperature, the suspensions were centrifuged, and the powders were collected and dried in an oven at 50–60°C. The adsorbed phosphate was sequentially extracted. One gram of each sample was weighed into a 50-mL centrifuge tube and then treated as described in Table 1.

Table 1.

2.5. Desorption of phosphate from loaded zeolites samples using bicarbonate solutions.

First, 0.5-g samples of phosphate-loaded zeolites (NaP1-FA and CaP1-NA) with phosphate contents ranging from 11 to 173 mmol/L were mixed with 20-mL solutions containing a mixture of $NaHCO_3$ (0.1 M) and Na_2CO_3 (0.1 M) in 50-mL plastic bottles. The bottles were mechanically shaken (Heidolph) at 21±1°C for 24 h at a constant agitation speed of 200 rpm. At the end of the experiment, the samples were withdrawn from the test bottles and filtered through a 0.45-µm membrane filter; the residual phosphate concentration was analysed using spectrophotometric colourimetry.

2.6. Physicochemical characterisation of zeolites

At the end of the sorption and desorption experiments, the zeolite samples were washed with water to remove the interstitial water and then oven-dried at 60°C for structural and textural analysis. The mineralogical composition was analysed by a Bruker D8 A25 Advance X-Ray Diffractometer θ-θ with $CuK_{\alpha 1}$ radiation, Bragg-Brentano geometry, and a linear LynxEyeXE detector. The diffractograms were obtained from 4º to 60º of 2θ with a step size of 0.015º and a counting time of 0.1 s as the sample rotated. The solids in powder form were identified by standard Joint Committee on Powder Diffraction Standards (JCPDS) files and were matched with Powder Diffraction Files (PDFs) no. 009-0077 for (brushite), no. 039-1374 (garronite), 039-0219 (NaP1), 046-1045 (quartz), and 015-0776 (mullite).

The samples' morphologies were examined by JEOL 3400 Field Emission Scanning Electron Microscopy with Energy Dispersive System FE-SEM-EDS prior gold metallisation.

The point of zero charge (PZC) values of NaP1-FA and CaP1-NA were determined, and the common intersection point (CIP) method was applied to the potentiometric titration curves obtained at four ionic strengths [28–30]. First, 0.1 g of zeolite was equilibrated with 25 mL of solutions with different ionic strengths (0.01-, 0.05-, 0.1-, and 0.5-M KNO_3) for 24 h at 200 rpm and 21±1°C. Following equilibration, a small quantity of 0.1-M KOH was added to the suspension to increase the pH beyond 10 (pHin). The suspension was then titrated with 0.0454-M HNO_3 to pH≈3 using an automatic titrator (Mettler Toledo). The net surface charge was correlated with the PZC determined from the titration data for the adsorbed amounts of [H^+] and [OH^-] ions.

Therefore, the titration curves of different ionic strength intersect at pH=pH_{PZC}. The surface charge was calculated according to Eq. 2 [31].

$$b = C_b - C_a + [H^+] - [OH^-] \quad (2)$$

where b (mol/g) is the net amount of hydroxide ions consumed; C_b and C_a (mol/L) are the base and acid concentrations, respectively; and [H^+] and [OH^-] denote the proton and hydroxide concentrations, respectively, calculated from the measured pH for a given mass of zeolite (g) and a given volume of solution (L). All measurements were performed in triplicate, and the average values are reported.

3. Results and discussion

3.1. Characterisation of the CaP1-NA modified zeolites.

The conversion of FA into zeolitic materials through the batch hydrothermal synthesis process involves three stages: i) the dissolution of Al and Si from FA, ii) the deposition of aluminosilicate gel on the FA surface, and iii) the crystallisation of zeolite from aluminosilicate gel [32]. The three Al- and Si-containing phases of the FA are i) amorphous aluminosilicate glass, ii) quartz, and iii) mullite. Aluminosilicate glass is the largest component and is the most unstable in the

hydrothermal environment, and therefore, it exhibits the highest rate of dissolution [33,34] makes the largest contribution to the produced zeolites.

The X-Ray Diffraction (XRD) patterns of the Na zeolite (NaP1-FA) and the synthesised Ca zeolite (CaP1-NA) are shown in Figure 1a. NaP1 ($Na_6(Al_6Si_{10}O_{32})\cdot 12H_2O$), mullite ($Al_2Si_2O_{13}$), and a trace of quartz (SiO_2) were the main phases identified in NaP1-FA. The XRD patterns of CaP1-NA indicated the presence of mullite, quartz, calcite ($CaCO_3$), and garronite ($NaCa_{2.5}(Si_{10}Al_6)O_{32}\cdot 14H_2O$) as the predominant phases. The SEM observation (Figure 1b) showed that NaP1-FA and CaP1-NA coat the FA. As shown in Figure 1b, the coating of NaP1-FA is not complete, as reported by Cama et al. [15].

Fig. 1.

The chemical compositions of both zeolitic materials are listed in Table 2 and indicate that NaP1-FA and CaP1-NA contained mainly Al_2O_3 and SiO_2, which accounted for a total of 74%. The synthesis of CaP1-NA considerably increased the Ca^{2+} content (from 1.4 to 7.4% (82.5 mg/g)). Accordingly, the Na^+ content decreased significantly (from 7.6 to less than 1%) because of treatment with $CaCl_2$ and the partial exchange of sodium and calcium ions in the zeolite structure.

Table 2.

The acid-base characterisation revealed pH_{PZC} values of 6.1±0.2 for CaP1-NA and 5.4±0.2 for NaP1-FA (Figure 2), which are in agreement with values reported for natural zeolites (clinoptilolite) (5.2±0.2) [35]. The increased pH_{PZC} of CaP1-NA suggests a decrease in the acidity of the metal-hydroxide groups (≅MOH) of the zeolite structure after modification with calcium-salts resulting from complexation with Ca(II) ions. The determined pH_{PZC} value is in agreement with values reported for α-$Al(OH)_3(s)$ (pH_{PZC}=5.0) and $Fe(OH)_3$ (pH_{PZC}=5–7).

Fig. 2.

Indeed, some studies [36–38] have reported that Fe- and Al-based surface groups on zeolites become positively charged and that their anion-sorption capacity (e.g., $H_2PO_4^-$/HPO_4^{2-}) via ligand exchange increase because of chemical interactions and electrostatic forces. The latter give rise to Columbic attraction or repulsion between binding sites and sorbing ions [39].

3.2. Phosphate-sorption capacities of CaP1-NA and NaP1-FA: Dependence on pH and phosphate concentration

The effects of the initial phosphate concentration on phosphate sorption and the equilibrium pH for both zeolites are shown in Figure 3a. The phosphate-sorption capacity increased as the initial phosphate concentration increased. Additionally, the equilibrium pH exceeds the initial pH (8), reaching values as high as 9.5 for CaP1-NA and 9 for NaP1-FA, at lower initial phosphate concentrations (up to 20 mmol/L) and then decreases back to the initial value for NaP1-FA and 7.5 for CaP1-NA. Moreover, the shape of the phosphate-sorption isotherm indicates that CaP1-NA has a higher affinity for phosphate than NaP1-FA, as shown by the higher slope of the isotherm. This high affinity results in the nearly quantitative removal of phosphate by CaP1-NA (98%) at low residual phosphate concentrations in solution. In contrast, for NaP1-FA, the removal ratios achieved were below 25% (data not shown). As the initial phosphate concentration was increased, the sorption capacities of the zeolites increased, reaching maxima of 207 mg/g and 50 mg/g for CaP1-NA and NaP1-FA, respectively (Figure .4).

Fig. 3.

According to the removal patterns exhibited by NaP1-FA and CaP1-NA zeolitic materials, the sorption of phosphate ions, mainly $H_2PO_4^-$ and HPO_4^{2-}, that occurs in the expected pH range (7 to 9) may follow two postulated mechanisms:

a) Surface complexation with ≅AlOH and ≅FeOH functional groups originally present as Al and Fe oxides or in the zeolitic structure via two main reactions:

a1) Outer-sphere complexes with $\cong MOH_2^+$ surface groups

$$\cong MOH_2^+ + H_2PO_4^-/HPO_4^{2-} \leftrightarrow \cong MOH_2^+ H_2PO_4^-/HPO_4^{2-} \quad (3)$$

a2) Inner-sphere complexes with $\cong MOH$ surface groups

$$\cong MOH + H_2PO_4^-/HPO_4^{2-} \leftrightarrow \cong MH_2PO_4^-/HPO_4^{2-} + OH^- \quad (4)$$

where M represents Al or Fe.

b) Formation of Ca-phosphate minerals with Ca(II) ions present on the zeolite through two main reactions:

b1) Ca-phosphate minerals with Ca(II) present on the zeolitic material as CaO(s) and $CaCO_3$(s):

$$H_2PO_4^-/HPO_4^{2-} + CaO(s)/CaCO_3\ (s) = \text{Ca-phosphate}\ (CaHPO_4(s) \text{ or } Ca_5(OH)(PO_4)_3(s)) \quad (5)$$

Both mineral phases can be formed in the expected pH range, as shown in Figure 5.4.

b2) Formation of Ca-phosphate minerals with Ca(II) ions occupying the ion-exchange groups of the zeolitic structure

$$(\cong ZO^-)_2Ca^{2+} + H_2PO_4^- + 2Na^+ \leftrightarrow 2\cong (ZO^-Na^+) + CaHPO_4(s) + H^+ \quad (6)$$

$$5(\cong ZO^-)_2Ca^{2+} + 3H_2PO_4^- + 10Na^+ \leftrightarrow 10\cong (ZO^-Na^+) + Ca_5(OH)(PO_4)_3\ (s)) + 7H^+ \quad (7)$$

where $\cong ZO^-$ represents the anionic groups of the zeolite structure.

The phosphate sorption that occurs via the formation of surface complexes (Eqs. 3–4) is consistent with the observed results at low phosphate concentrations (Figure 3b), which involved the removal of $H_2PO_4^-$ (Eq. 3) and the formation of inner-sphere complexes (Eq. 4). For high initial phosphate concentrations (50–200 mmol/L), the most favoured reaction is the formation of Ca-phosphate (e.g., brushite or Hap) (Eqs. 6–7) with the release of H^+ ions and the resulting

decrease in the pH to 7.5 for CaP1-NA. For NaP1-FA, the lower Ca(II) content results in a lower sorption capacity, and thus, the recovery of phosphate ions should be conceived of as a combination of Eqs. 3–6. XRD analysis of the samples after the sorption experiments revealed the presence of brushite in most of the analysed CaP1-NA samples, while for NaPa1-NA, the presence of Ca-phosphate minerals was not observed. This could be attributable to the contents of these minerals on the samples being below the limit of detection or the formation of the minerals within the small channels of the zeolite as undetectable nanocrystals.

The formation of Ca-phosphate (brushite and Hap) is thermodynamically favoured in the expected pH range, as shown in Figure S1 (Supplementary material). Hap is more stable than brushite, which is considered its precursor phase. However, as the reaction proceeds on the microporous zeolite structure, brushite is formed and then stabilised, thereby stopping the conversion to Hap.

The phosphate-sorption isotherms of CaP1-NA and NaP1-FA at different pH values (7, 8, and 9) are shown in Figure 4. The phosphate-loading capacity of CaP1-NA is higher than that of NaP1-FA; e.g., 203±11 mg/g compared with 57±5 mg/g at pH 8. The larger sorption capacity of CaP1-NA is associated with its Ca content and high availability for reaction, mainly at the ion-exchange sites, while the lower sorption capacity of NaP1-FA is related to unreacted Ca in the form of CaO. It should be mentioned that the initial S_{BET} increased during zeolite modification from 6.3 to 13.6 m^2/g. Thus, the higher Ca content and larger surface area enhance the phosphate sorption, as previously reported [40]. The surface charge properties of the active sites (Fe and Al sites) of both zeolites were 8% Al and 2.5% Fe (Table 2). The larger amount of Al in NaP1-FA plays an important role in phosphate removal at neutral pH, and the magnitude of the Columbic attractive force decreases as the active sites become neutral.

The sorption isotherm data were fitted using Langmuir (Eq. 7) and Freundlich isotherm models (Eq. 8):

$$\frac{C_e}{q_e} = \frac{1}{K_l q_m} + \frac{C_e}{q_m} \quad (7)$$

$$\log q_e = \log K_f + \frac{1}{n} \log C_e \quad (8)$$

where C_e (mg/L) and q_e (mg/g) are the equilibrium total phosphate concentrations in the aqueous and solid phases, respectively; q_m (mg/g) is the maximum sorption capacity; K_L (L/mg) is the Langmuir sorption equilibrium constant; n is a constant indicating the Freundlich isotherm curvature; and K_f ((mg/g)/(mg/L)^n) is the Freundlich equilibrium constant. The sorption parameters and regression coefficients (R^2) obtained from the linear regression of Eqs. 7 and 8 are listed in Table 3.

The experimental and predicted sorption isotherm data by the Langmuir model at different pH values for the CaP1-NA and NaP1-FA zeolites are shown in Figure 4.

Fig. 4.

Table 3.

The phosphate-removal data for CaP1-NA were well described by the Langmuir isotherm, while for NaP1-FA, the Freundlich isotherm was more suitable. This behaviour was explained by Pengthamkeerati et al. [41], who reported that the phosphate-adsorption processes of zeolite derived from FA using different treatment methods can be described using different isotherm models. Langmuir isotherm is more suitable for the adsorption pattern of phosphate on the alkaline-treated and Ca-rich zeolite CaP1-NA. In contrast, the Freundlich isotherm better describes physical adsorption, and as a result, this model is suitable for the phosphate-adsorption pattern of NaP1-FA.

The XRD patterns of phosphate-loaded CaP1-NA samples with initial phosphate concentrations ranging from 8 to 15 g/L at pH values of 7, 8, and 9 are shown in Figure 5. These patterns revealed the formation of Ca-phosphate in the form of brushite ($CaPO_3(OH).2H_2O(s)$) as the

major phase at pH 7 and 8 and as a minor phase at pH 9. Similar phosphate-removal and brushite-formation results were reported by Pengthamkeerati et al. [41] with Ca-zeolites and by other researchers (e.g. Lu et al., and Xu et al) [42,43] with FA. The formation of brushite instead of Hap is associated with the prevalence of kinetic control. In fact, the reactive crystallisation of brushite has been described to occur [44,45] through five successive stages: (i) spontaneous Hap precipitation, (ii) complete dissolution of Ca and Hap growth, (iii) initial appearance of brushite nuclei, (iv) coexistence of Hap and brushite, and (v) transformation of Hap into brushite and subsequent brushite growth.

Fig. 5.

The transformation of Hap into brushite would not be expected because Hap is the most thermodynamically stable species. Nevertheless, under the conditions, Hap appears to be in a low-crystallinity state and in metastable equilibrium with brushite, whose faster crystal growth drives the transformation.

Both zeolites exhibit maximum sorption capacities at pH 8, which slightly decrease as the pH increases to 9 or decreases to 7. This pH-dependent sorption behaviour is in agreement with the brushite formation observed in most of the samples analysed by XRD (Figure 5). The logarithmic solubility dependence of brushite and the phosphate-loading capacity as a function of pH are plotted in Figure 6. The minimum solubility corresponding the highest brushite stability occurs at pH 8 (maximum loading capacity) and decreases slightly as the pH is decreased to pH 7 or increased to 9.

Fig. 6.

Similar behaviour was observed for NaP1-FA, the maximum sorption capacities were observed at pH 8 and 7 and were slightly reduced when the pH increased to 9, which could be in agreement

with the potential involvement of the CaO(s) present on the zeolite in brushite formation and the acid-base properties of the ≅AlOH and ≅FeOH surface groups, which exhibit pH_{pcz} of approximately 6 for hydrated Al oxides [46] and 7 for hydrated Fe oxides. As a result, at basic pH values exceeding the pH_{pcz}, the formation of outer-sphere complexes will be negligible. Additionally, in alkaline conditions, the formation of inner-sphere complexes is not favoured, and thus, the removal ratio decreases.

The phosphate-sorption capacities of zeolites and FA as reactive materials for phosphate removal are compared in Table 4, which shows that the phosphate-sorption capacities of CaP1-NA exceed previously reported values.

Table 4.

3.3. P speciation of the phosphate in loaded CaP1-NA/NaP1-FA

The speciation results of CaP1-NA and NaP1-FA zeolitic materials are shown in Figure 7. The easily exchangeable speciation (KCl-P) associated with exchange reactions as defined by Eq. 3 accounts for up to 20% for NaP1-FA and less than 10% for CaP1-NA. The dissolved species obtained using NaOH solutions (NaOH-P) reveal that the P bound to the hydrated metal oxides (the inner-sphere and outer-sphere complexes described by Eqs. 3–4) makes only a small contribution for NaP1-FA (less than 5%) and no contribution for CaP1-NA. In NaOH solutions, the ≅MOH^{2+} and ≅MOH groups are deprotonated, and the excess OH ions disrupt the ≅$MH_2PO_4^-$ /HPO_4^{2-}complexes. The HCl-P speciation (was in line with laboratory experiments reported by other researchers (e.g. Wang et al. And Meis et al., [47,48])) associated with Ca-phosphate mineral phases (brushite and Hap) accounts for up to 80% for NaP1-FA and more than 90% for CaP1-NA. The species produced by the residual speciation contributed less than 1% for both zeolites.

Fig. 7.

3.4. Effect of competing ions on phosphate sorption

Coexisting ions, such as chloride, sulfate, nitrate, and carbonate, that are generally present in treated wastewater do not interfere with phosphate uptake through competitive sorption, as shown in Figure 8. Differences between the samples containing individual species, mixtures of species, and no coexisting ions are not statistically significant. Given that the main phosphate-removal mechanism is based on the formation of insoluble Ca-phophate minerals and weak complexes with MOH surface groups, none of the evaluated anions could form insoluble forms with Ca anions, and their complexation with Fe and Al oxides was also less favoured than that with phosphate anions. According to Zhang et al. [49], this can be attributed to the specific sorption of phosphate on the adsorbent because the phosphate ions adsorbed on the strongly specific sites were rarely exchangeable, even in solutions containing excessive amounts of coexisting ions. This suggests that CaP1-NA has high sorption selectivity for phosphate anions and great potential for use in treated wastewater expected to contain high concentrations of theses anions.

Fig. 8.

3.5. Desorption of phosphate from loaded zeolite samples

The phosphate desorption achieved using 0.1 mol/L $NaHCO_3/Na_2CO_3$ solutions increased as the amount of phosphate on the zeolitic material decreased (Figure 9a-b). Partial desorption (30 to 70%) was reported for CaP1-NA, whereas values of 10 to 70% were observed for NaP1-FA in a single-extraction trial. These results are in agreement with the speciation results obtained in using excess bicarbonate ions. Indeed, during labile speciation (P-KCl), phosphate anions will be displaced by bicarbonate ions, and partial brushite dissolution will be achieved, as indicated in Figure 6, which shows that increasing the pH increases the solubility of brushite by up to one order of magnitude. It can be concluded that phosphate sorption on CaP1-NA is relatively

irreversible and that the bonding between the actives sites and the adsorbed phosphate is quite strong.

Fig. 9.

4. Conclusions

NaP1-FA zeolitic material synthesised from Narcea FA and its Ca-modified form (CaP1-NA) are capable of high phosphate sorption in neutral to slightly basic conditions. The maximum phosphate-sorption capacities determined at pH 8 were 65±7 and 203±11 mgP-PO4/g zeolite for NaP1-FA and CaP1-NA, respectively. The sorption capacity in the expected pH range of wastewater effluents (e.g., from 7 to 9) was slightly dependent on the pH and was maximised at pH 8 for CaP1-NA and pH 9 for NaP1-FA. Phosphate removal by NaP1-FA occurred via a surface complexation mechanism involving the AlOH and FeOH surface groups of the unreacted Fe and Al oxides originally present on the FA or the potential formation of Ca-phosphate phases using the original CaO present on the FA. In contrast, for CaP1-NA, the main removal mechanism included the formation of a Ca-phosphate, brushite, as confirmed by XRD analyses. The higher solubility of brushite compared with that of Hap makes this zeolitic material promising as a novel inorganic zeolite/CaP1-NA/brushite fertiliser.

Acknowledgments

This study has been supported by the Waste2Product project (CTM2014-57302-R) financed by Ministry of Science and Innovation (MINECO, Spain) and the Catalan government (project ref. 2014SGR050). Authors acknowledge R. Estany (Aigues de Barcelona) and M. Gullom (EMMA) and I. Sancho (Centro Tecnologíco del Agua (CETAQUA)) for treated wastewater samples supply.

References

1. Yao, Z. T. *et al.* A comprehensive review on the applications of coal fly ash. *Earth-Science Rev.* **141,** 105–121 (2015).

2. Blissett, R. S. & Rowson, N. A. A review of the multi-component utilisation of coal fly ash. *Fuel* **97,** 1–23 (2012).

3. Singer, P. a., Salamanca-Buentello, F. & Daar, A. S. Harnessing nanotechnology to improve global equity. *Issues Sci. Technol.* **21,** 57–64 (2005).

4. Xie, J., Wang, Z., Wu, D., Zhang, Z. & Kong, H. Synthesis of Zeolite/Aluminum Oxide Hydrate from Coal Fly Ash: A New Type of Adsorbent for Simultaneous Removal of Cationic and Anionic Pollutants. *Ind. Eng. Chem. Res.* **52,** 14890–14897 (2013).

5. Yang, M., Lin, J., Zhan, Y. & Zhang, H. Adsorption of phosphate from water on lake sediments amended with zirconium-modified zeolites in batch mode. *Ecol. Eng.* **71,** 223–233 (2014).

6. Zhou, L., Chen, Y. L., Zhang, X. H., Tian, F. M. & Zu, Z. N. Zeolites developed from mixed alkali modified coal fly ash for adsorption of volatile organic compounds. *Mater. Lett.* **119,** 140–142 (2014).

7. Querol, X. *et al.* Synthesis of zeolites from coal fly ash□: an overview. **50,** 413–423 (2002).

8. Ansari, M., Aroujalian, A., Raisi, A., Dabir, B. & Fathizadeh, M. Preparation and characterization of nano-NaX zeolite by microwave assisted hydrothermal method. *Adv. Powder Technol.* **25,** 722–727 (2014).

9. Hollman, G., Steenbruggen, G. & Janssen-Jurkovičová, M. A two-step process for the synthesis of zeolites from coal fly ash. *Fuel* **78,** 1225–1230 (1999).

10. Moreno, N. *et al.* Potential Environmental Applications of Pure Zeolitic Material Synthesized from Fly Ash. *J. Environ. Eng.* **127,** 994–1002 (2001).

11. Desmidt, E. *et al.* Global phosphorus scarcity and full-scale P-recovery techniques-a review. *Crit. Rev. Environ. Sci. Technol.* 336–384 (2013).

12. Boyer, T. H., Persaud, A., Banerjee, P. & Palomino, P. Comparison of low-cost and engineered materials for phosphorus removal from organic-rich surface water. *Water Res.* **45,** 4803–4814 (2011).

13. Querol, X. *et al.* Synthesis of high ion exchange zeolites from coal fly ash. *Geol. Acta* **5,** 49–57 (2007).

14. Moreno, N., Querol, X., Ayora, C., Pereira, C. F. & Janssen-Jurkovicová, M. Utilization of zeolites synthesized from coal fly ash for the purification of acid mine waters. *Environ. Sci. Technol.* **35,** 3526–34 (2001).

15. Cama, J., Ayora, C., Querol, X. & Ganor, J. Dissolution kinetics of synthetic zeolite NaP1 and its implication to zeolite treatment of contaminated waters. *Environ. Sci. Technol.* **39,** 4871–7 (2005).

16. Watanabe, Y. *et al.* Preparation of a zeolite NaP1/hydroxyapatite nanocomposite and study of its behavior as inorganic fertilizer. *J. Chem. Technol. Biotechnol.* **89,** 963–968 (2014).

17. Golden, D. C. & Ming, D. W. Division s-9-soil mineralogy. **664,** 657–664 (1999).

18. Liu, R. & Lal, R. Synthetic apatite nanoparticles as a phosphorus fertilizer for soybean (Glycine max). *Sci. Rep.* **4,** 1–6 (2014).

19. Liu, X. & Ding, C. Morphology of apatite formed on surface of wollastonite coating soaked in simulate body fluid. *Mater. Lett.* **57,** 652–655 (2002).

20. Watanabe, Y. *et al.* Formation of hydroxyapatite nanocrystals on the surface of Ca-Al-layered double hydroxide. *J. Am. Ceram. Soc.* **93,** 1195–1200 (2010).

21. Zhou, J. Z. *et al.* Efficient and controllable phosphate removal on hydrocalumite by multi-step treatment based on pH-dependent precipitation. *Chem. Eng. J.* **185-186,** 219–225 (2012).

22. Dorozhkin, S. V. Self-Setting Calcium Orthophosphate Formulations: Cements, Concretes, Pastes and Putties. *Int. J. Mater. Chem.* **1,** 1–48 (2012).

23. Parvinzadeh Gashti, M., Stir, M., Bourquin, M. & Hulliger, J. Mineralization of Calcium Phosphate Crystals in Starch Template Inducing a Brushite Kidney Stone Biomimetic Composite. *Cryst. Growth Des.* **13,** 2166–2173 (2013).

24. Kitson, R.E; Mellon, M. . Colorimetric determination of phosphorus as molybdovanadophosphoric acid. *Ind. Eng. Chem.* (1944).

25. M.J.Hedley, J.W. B Stewart, B. S. C. Changes in Inorganic and Organic Soil Phosphorus Fractions Induced by Cultivation Practices and by Laboratory Incubations. *Soil.Sci.AM.J* **46,** 970–976 (1982).

26. Ann, Y., Reddy, K. R. & Delfino, J. J. Influence of chemical amendments on phosphorus immobilization in soils from a constructed wetland. **14,** 157–167 (2000).

27. Moharami, S. & Jalali, M. Phosphorus leaching from a sandy soil in the presence of modified and un-modified adsorbents. *Environ. Monit. Assess.* **186,** 6565–76 (2014).

28. Skartsila, K. & Spanos, N. Surface characterization of hydroxyapatite: Potentiometric titrations coupled with solubility measurements. *J. Colloid Interface Sci.* **308,** 405–412 (2007).

29. Liu, Y., Naidu, R. & Ming, H. Surface electrochemical properties of red mud (bauxite residue): zeta potential and surface charge density. *J Colloid Interface Sci* **394,** 451–457 (2013).

30. Zebardast, H. R., Pawlik, M., Rogak, S. & Asselin, E. Potentiometric titration of hematite and magnetite at elevated temperatures using a ZrO2-based pH probe. *Colloids Surfaces A Physicochem. Eng. Asp.* **444,** 144–152 (2014).

31. Martinez, R. E., Pokrovsky, O. S., Schott, J. & Oelkers, E. H. Surface charge and zeta-potential of metabolically active and dead cyanobacteria. *J. Colloid Interface Sci.* **323,** 317–325 (2008).

32. Murayama, N., Yamamoto, H. & Shibata, J. Zeolite synthesis from coal fly ash by hydrothermal reaction using various alkali sources. *J. Chem. Technol. Biotechnol.* **77,** 280–286 (2002).

33. Poole, C., Prijatama, H., and Rice, N.M. Synthesis of zeolite adsorbents by hydrothermal treatement of PFA wastes: A comparative study. *Miner. Eng.* **13,** 831–842 (2000).

34. Querol, X. *et al.* Synthesis of zeolites from fly ash at pilot plant scale. *Fuel* **80,** 857–865 (2001).

35. Guaya, D., Valderrama, C., Farran, A., Armijos, C. & Cortina, J. L. Simultaneous phosphate and ammonium removal from aqueous solution by a hydrated aluminum oxide modified natural zeolite. *Chem. Eng. J.* **271,** 204–213 (2015).

36. Zhang, B.-H. *et al.* Simultaneous removal of ammonium and phosphate by zeolite synthesized from coal fly ash as influenced by acid treatment. *J. Environ. Sci. (China)* **19,** 540–5 (2007).

37. Reed, B.B.E., Vaughan, R., Jiang, L. As (III), As (V), Hg and removal by Fe-Oxide impregnated activated carbon. 869–873 (2000).

38. Chen, J. *et al.* Removal of phosphate from aqueous solution by zeolite synthesized from fly ash. *J. Colloid Interface Sci.* **300,** 491–7 (2006).

39. Onyango, M. S., Kuchar, D., Kubota, M. & Matsuda, H. Adsorptive removal of phosphate ions from aqueous solution using synthetic zeolite. *Ind. Eng. Chem. Res.* **46,** 894–900 (2007).

40. Ji, X. *et al.* Immobilization of ammonium and phosphate in aqueous solution by zeolites synthesized from fly ashes with different compositions. *J. Ind. Eng. Chem.* **22,** 1–7 (2014).

41. Pengthamkeerati, P., Satapanajaru, T. & Chularuengoaksorn, P. Chemical modification of coal fly ash for the removal of phosphate from aqueous solution. *Fuel* **87,** 2469–2476 (2008).

42. Lu, S. G., Bai, S. Q., Zhu, L. & Shan, H. D. Removal mechanism of phosphate from aqueous solution by fly ash. *J. Hazard. Mater.* **161,** 95–101 (2009).

43. Xu, K., Deng, T., Liu, J. & Peng, W. Study on the phosphate removal from aqueous solution using modified fly ash. *Fuel* **89,** 3668–3674 (2010).

44. Oliveira, C., Georgieva, P., Rocha, F., Ferreira, A. & Feyo de Azevedo, S. Dynamical model of brushite precipitation. *J. Cryst. Growth* **305,** 201–210 (2007).

45. Ferreira, A., Oliveira, C. & Rocha, F. The different phases in the precipitation of dicalcium phosphate dihydrate. *J. Cryst. Growth* **252,** 599–611 (2003).

46. Simsek, E. B., Özdemir, E. & Beker, U. Zeolite supported mono- and bimetallic oxides: Promising adsorbents for removal of As(V) in aqueous solutions. *Chem. Eng. J.* **220,** 402–411 (2013).

47. Wang, C., Qi, Y. & Pei, Y. Laboratory investigation of phosphorus immobilization in lake sediments using water treatment residuals. *Chem. Eng. J.* **209,** 379–385 (2012).

48. Meis, S., Spears, B. M., Maberly, S. C., O'Malley, M. B. & Perkins, R. G. Sediment amendment with Phoslock?? in Clatto Reservoir (Dundee, UK): Investigating changes in sediment elemental composition and phosphorus fractionation. *J. Environ. Manage.* **93,** 185–193 (2012).

49. Zhang, G., Liu, H., Liu, R. & Qu, J. Removal of phosphate from water by a Fe-Mn binary oxide adsorbent. *J. Colloid Interface Sci.* **335,** 168–74 (2009).

50. Xie, J., Wang, Z., Fang, D., Li, C. & Wu, D. Green synthesis of a novel hybrid sorbent of zeolite/lanthanum hydroxide and its application in the removal and recovery of phosphate from water. *J. Colloid Interface Sci.* **423,** 13–19 (2014).

51. Xie, J., Wang, Z., Wu, D. & Kong, H. Synthesis and properties of zeolite/hydrated iron oxide composite from coal fly ash as efficient adsorbent to simultaneously retain cationic and anionic pollutants from water. *Fuel* **116,** 71–76 (2014).

52. Zhang, M. *et al.* Removal of Phosphate from Aqueous Solution Using Zeolite Synthesized from Fly Ash by Alkaline Fusion Followed by Hydrothermal Treatment. *Sep. Sci. Technol.* **46,** 2260–2274 (2011).

53. Wu, D., Zhang, B., Li, C., Zhang, Z. & Kong, H. Simultaneous removal of ammonium and phosphate by zeolite synthesized from fly ash as influenced by salt treatment. *J. Colloid Interface Sci.* **304,** 300–306 (2006).

54. Chmielewská, E., Hodossyová, R. & Bujdoš, M. Kinetic and thermodynamic studies for phosphate removal using natural adsorption materials. *Polish J. Environ. Stud.* **22,** 1307–1316 (2013).

55. Puigdomènech, I. Chemical Equilibrium Software Hydra and Medusa. *Inorganic Chemistry Department* Stock. Sweden (2001).

Table 1. Chemical extraction scheme for phosphate speciation of loaded zeolites

Reagent conditions	Speciation name	Speciation (associated phosphate forms)	Step
40-mL 2 M KCl for 2h	KCl-P	Soluble and exchangeable P	1
40-mL 0.1 M NaOH for 17h	NaOH-P	Fe- and Al-bound P	2
40-mL 0.5 M HCl for 24h	HCl-P	Ca-bound P	3
40 ml 8 M HNO_3/5 M $HClO_4$	Res-P	Residual P	4

Table 2. Average chemical composition of zeolitic adsorbents NaP1-FA and CaP1-NA by using FSEM-EDX

	SiO_2	Al_2O_3	Fe_2O_3	Na_2O	CaO	K_2O	P_2O_5	MgO
NaP1-FA (%)	48.3	22.5	6.1	15.2	3.0	3.3	1.3	1.2
CaP1-NA (%)	47.8	23.3	5.7	2.0	15.8	3.0	1.53	1.4

[1.] Composition values have been expressed as oxide forms.

Table 3. Langmuir and Freundlich isotherm parameters for CaP1-NA and NaP1-FA at different pH.

Adsorbent		CaP1-NA			NaP1-FA		
Adsorption isotherm models		pH 7	pH 8	pH 9	pH 7	pH 8	pH 9
Langmuir equation	q_m	192	203.6	153	55.9	57.3	43.3
	K_L	0,004	0.004	0.006	0.0006	0.00035	0.0004
	R^2	0,86	0.99	0.96	0.82	0.90	0.91
Freundlich equation	K_f	1.45	14.8	17.6	2.23	0.0065	0.81
	n	1.36	3.4	2.9	3.01	1.17	2.48
	R^2	0.96	0.78	0.93	0.88	0.93	0.98

Table 4. Comparison of phosphate sorption capacity for different materials based Zeolite and FA

Material	q_m (mg/g)	pH	Reference
Zeolite NaP1-FA	57.33	8	This study
Calcium modified Zeolite NaP1-FA (CaP1-NA)	203.6	8	This study
Zeolite/Lanthanum hydroxide (La-ZFA)	71.94	>9.24	50
Zeolite/hydrate iron oxide (ZFA/Fe_2O_3)	18.2	6.6	51
Zeolite synthesized from fly ash by alkaline fusion	132, 157,184.	7	52
NaOH treated fly ash (TFA-NaOH)	57.14	8-12	41
Calcium modified Zeolite NaP1/hydroxyapatite	24.1	9	16
Fly ashes from three coal-burning power plants	90, 91, 108	11,11,12	42
Synthesis zeolite –Ca	30.46	6.78	53
Natural zeolite (Clinoptilolite)	13.8	n.a	54

n.a = not available

Figure captions:

Fig. 1. (a) XRD patterns of NaP1-NA and its modified zeolite CaP1-NA and (b) SEM: NaP1-NA and CaP1-NA.

Fig. 2. Potentiometric titration curve, at 0.01, 0.05, 0.1, and 0.5 M KNO_3 for Zeolite: a) CaP1-NA and b) NaP1-NA.

Fig. 3. (a) The equilibrium pH evolution as a function of initial phosphate concentration (initial pH 8) for CaP1-NA and NaP1-NA zeolitic material and (b) the uptake concentration as a function of equilibrium adsorbed concentration.

Fig. 4. Phosphate sorption isotherms at different pH and predicted uptake by the Langmuir (left) and Freundlich (right) isotherms for (a-b) CaP1-NA and (c-d) NaP1-NA modified zeolitic material.

Fig. 5. XRD pattern after phosphate sorption by CaP1-NA zeolitic material modified and brushite formation at different pH.

Fig. 6.The experimental P(V) sorption capacity at different pH and the estimated curve of brushite solubility for the CaP1-NA isotherm.

Fig. 7. Phosphate speciation of the NaP1-NA and CaP1-NA with initial amount of phosphate in equilibrium (q_e = 12±1 mg/g).

Fig. 8. Effect of coexisting anions on phosphate recovery at different initial phosphate concentration with fixed and mixed anions (Cl^- = 300 mg/L; SO_4^{2-} = 250mg/L; NO^{3-} = 50 mg/L; HCO^{3-} = 300 mg/L).

Fig. 9. Phosphate desorption using mixture of $NaHCO_3$ (0.1M) and Na_2CO_3 (0.1 M) from loaded zeolite (a) CaP1-NA and (b) NaP1-NA.

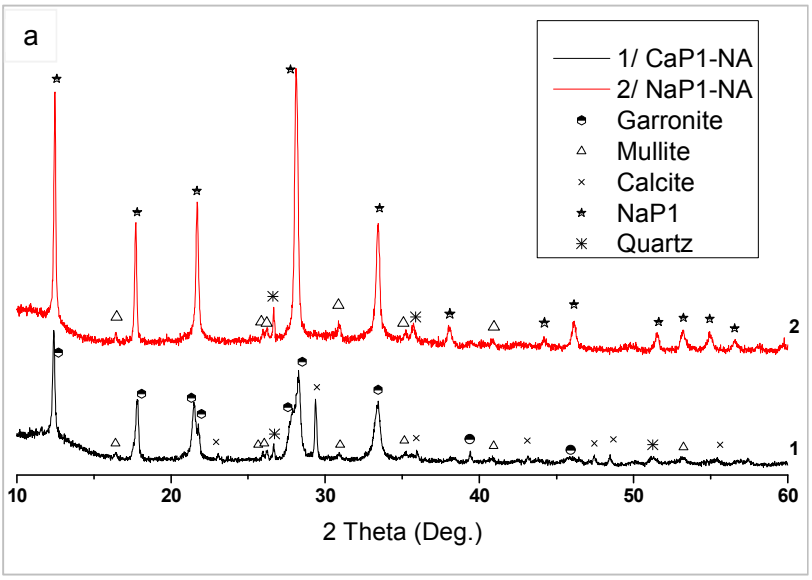
a
1/ CaP1-NA
2/ NaP1-NA
Garronite
Mullite
Calcite
NaP1
Quartz
2
1
10
20
30
40
50
60
2 Theta (Deg.)

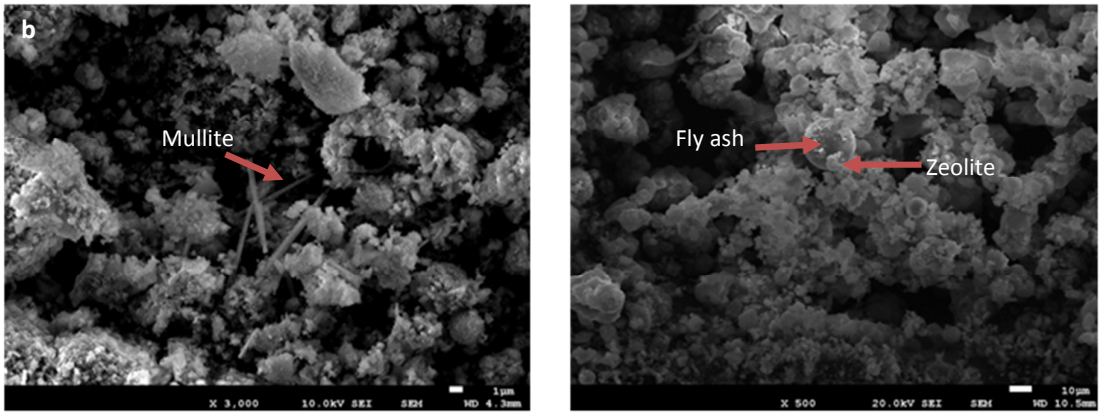
b
Mullite
Fly ash
Zeolite

Fig. 1.

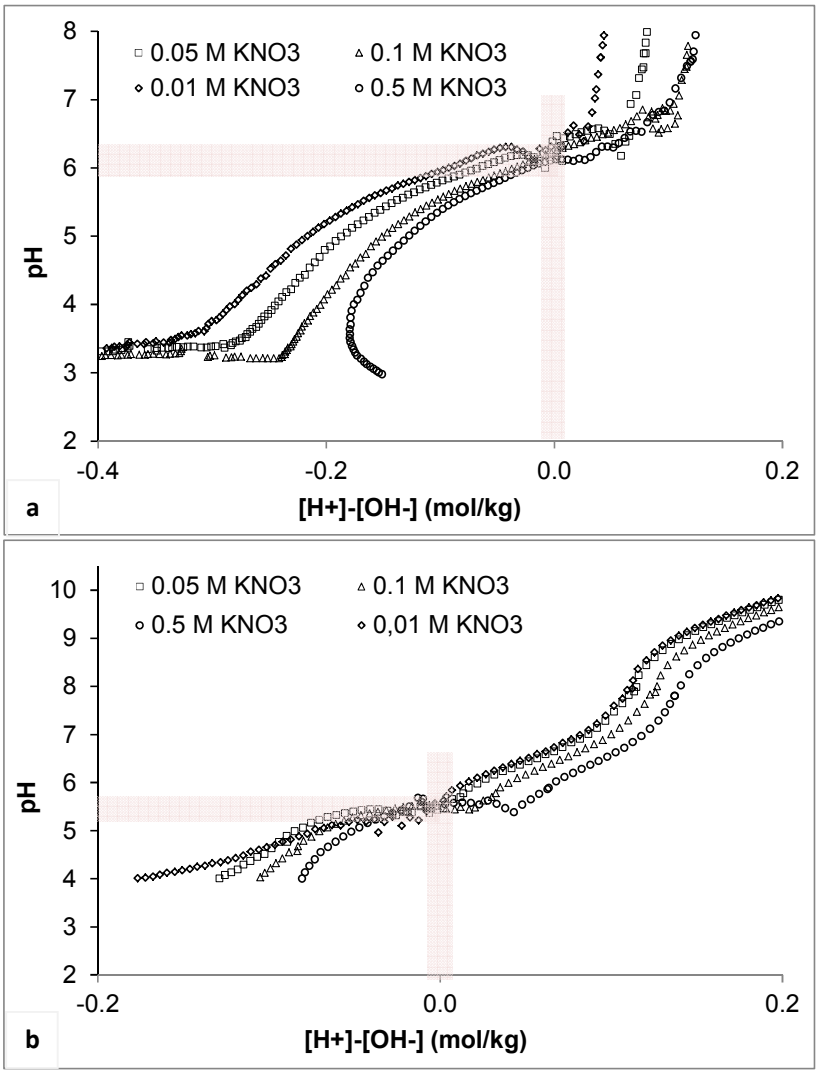
0.05 M KNO3
0.1 M KNO3
0.01 M KNO3
0.5 M KNO3
pH
[H+]-[OH-] (mol/kg)
a
0.05 M KNO3
0.1 M KNO3
0.5 M KNO3
0,01 M KNO3
pH
[H+]-[OH-] (mol/kg)
b

Fig. 2.

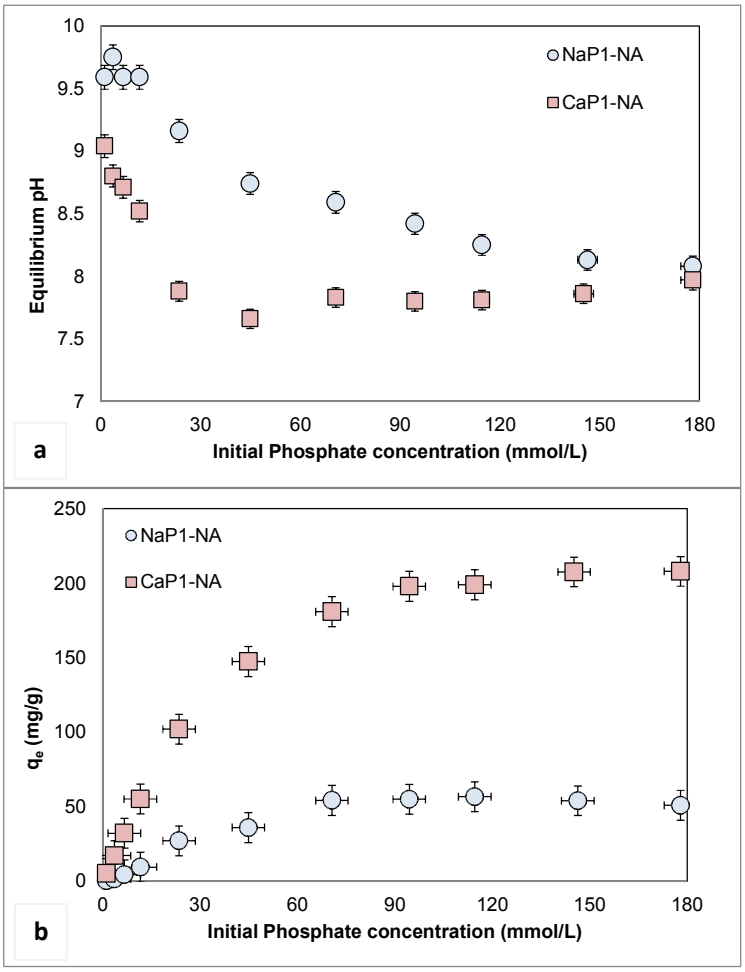
NaP1-NA
CaP1-NA
Equilibrium pH
Initial Phosphate concentration (mmol/L)
a
NaP1-NA
CaP1-NA
q_e (mg/g)
Initial Phosphate concentration (mmol/L)
b

Fig. 3.

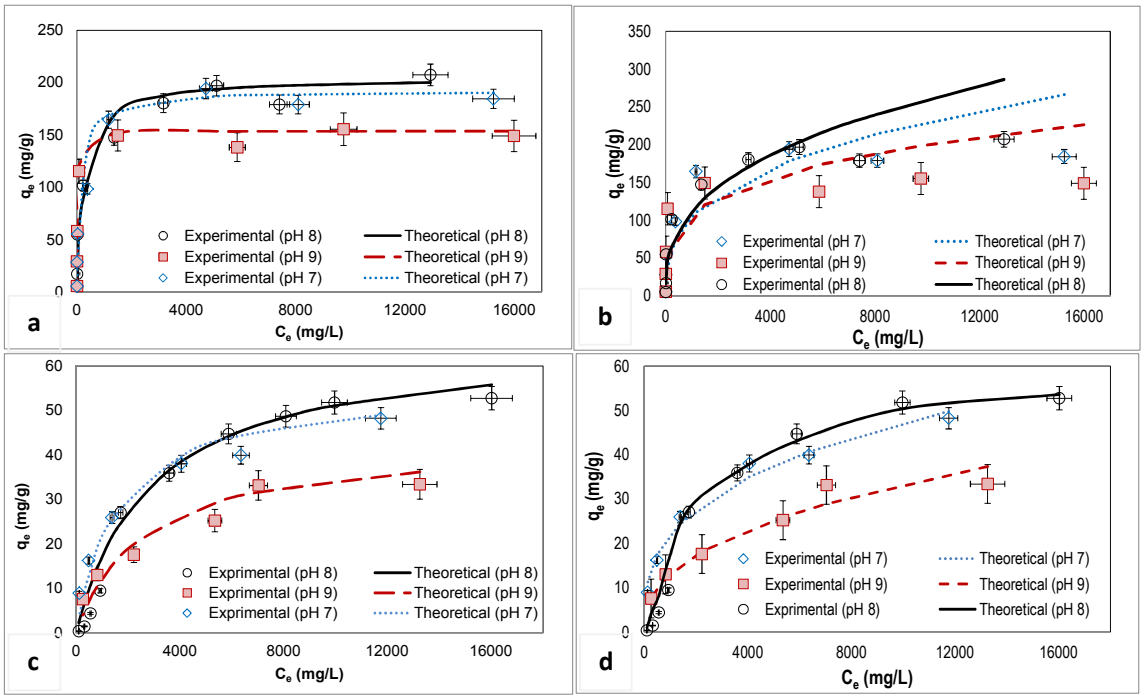
a
q_e (mg/g)
C_e (mg/L)
Experimental (pH 8)
Experimental (pH 9)
Experimental (pH 7)
Theoretical (pH 8)
Theoretical (pH 9)
Theoretical (pH 7)
b
q_e (mg/g)
C_e (mg/L)
Experimental (pH 7)
Experimental (pH 9)
Experimental (pH 8)
Theoretical (pH 7)
Theoretical (pH 9)
Theoretical (pH 8)
c
q_e (mg/g)
C_e (mg/L)
Exprimental (pH 8)
Exprimental (pH 9)
Exprimental (pH 7)
Theoretical (pH 8)
Theoretical (pH 9)
Theoretical (pH 7)
d
q_e (mg/g)
C_e (mg/L)
Experimental (pH 7)
Experimental (pH 9)
Exprimental (pH 8)
Theoretical (pH 7)
Theoretical (pH 9)
Theoretical (pH 8)

Fig. 4.

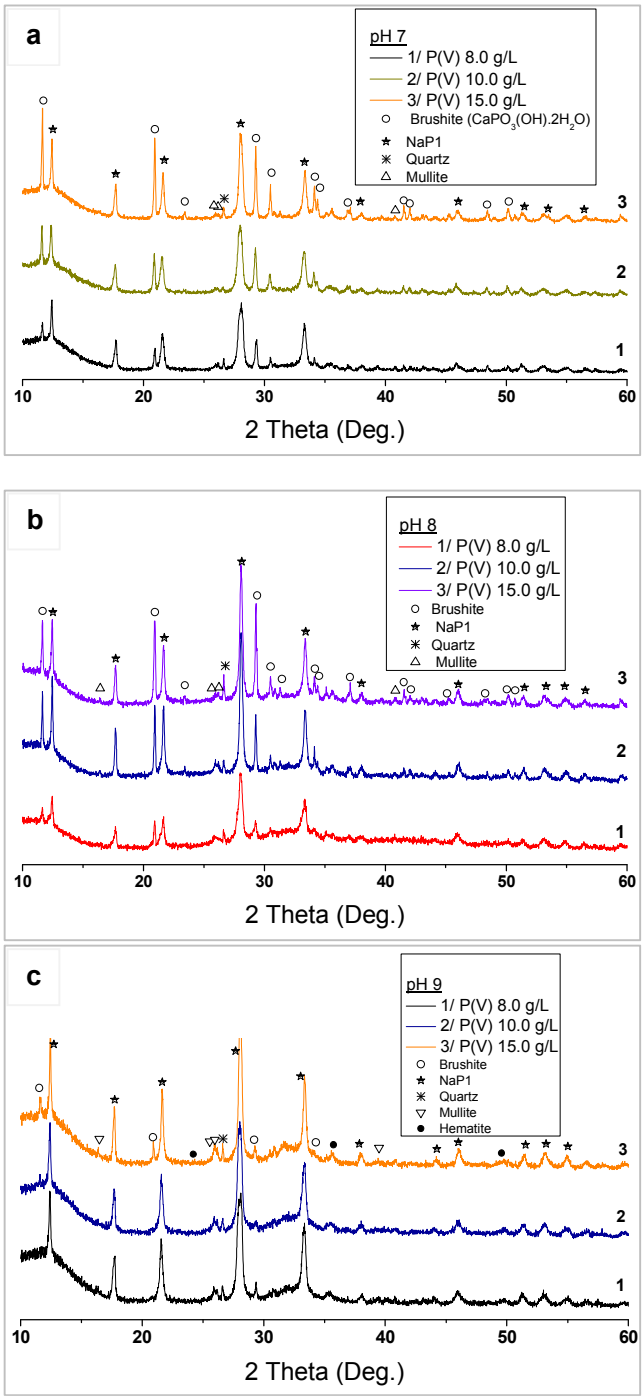
a
pH 7
1/ P(V) 8.0 g/L
2/ P(V) 10.0 g/L
3/ P(V) 15.0 g/L
Brushite (CaPO3(OH).2H2O)
NaP1
Quartz
Mullite
3
2
1
10
20
30
40
50
60
2 Theta (Deg.)
b
pH 8
1/ P(V) 8.0 g/L
2/ P(V) 10.0 g/L
3/ P(V) 15.0 g/L
Brushite
NaP1
Quartz
Mullite
3
2
1
10
20
30
40
50
60
2 Theta (Deg.)
c
pH 9
1/ P(V) 8.0 g/L
2/ P(V) 10.0 g/L
3/ P(V) 15.0 g/L
Brushite
NaP1
Quartz
Mullite
Hematite
3
2
1
10
20
30
40
50
60
2 Theta (Deg.)

Fig. 5.

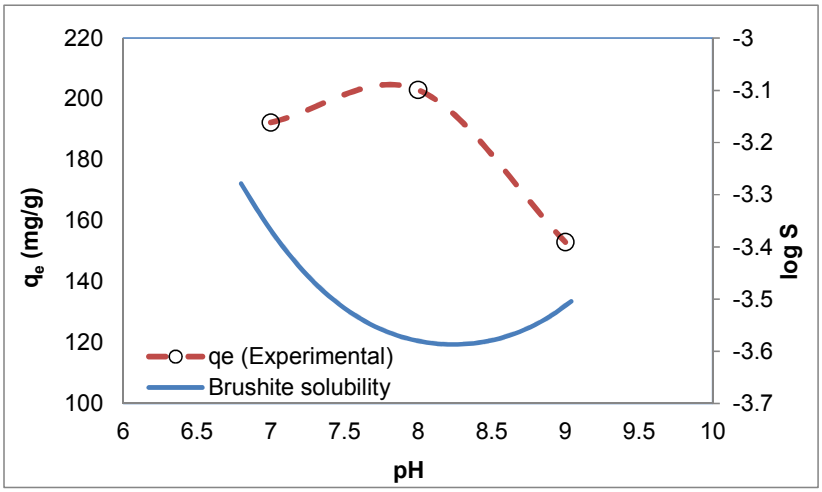
220
200
180
160
140
120
100
-3
-3.1
-3.2
-3.3
-3.4
-3.5
-3.6
-3.7
6
6.5
7
7.5
8
8.5
9
9.5
10
pH
qe (mg/g)
log S
qe (Experimental)
Brushite solubility

Fig. 6.

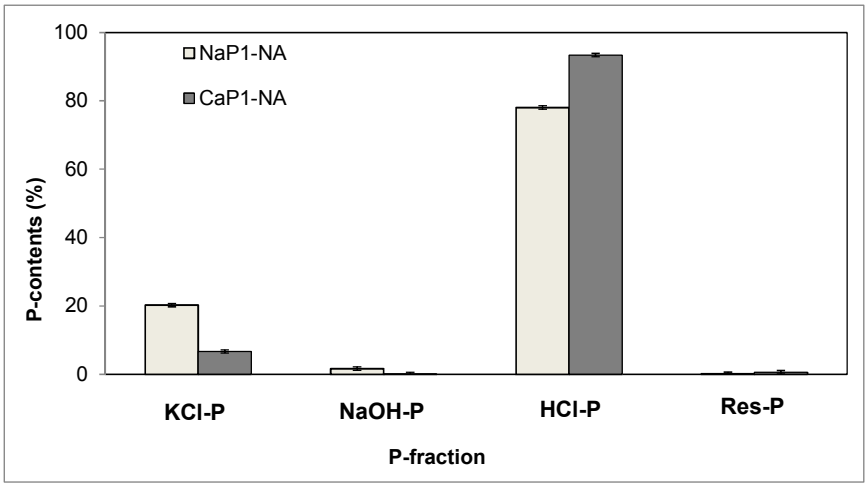
100
80
60
40
20
0
P-contents (%)
NaP1-NA
CaP1-NA
KCl-P
NaOH-P
HCl-P
Res-P
P-fraction

Fig. 7.

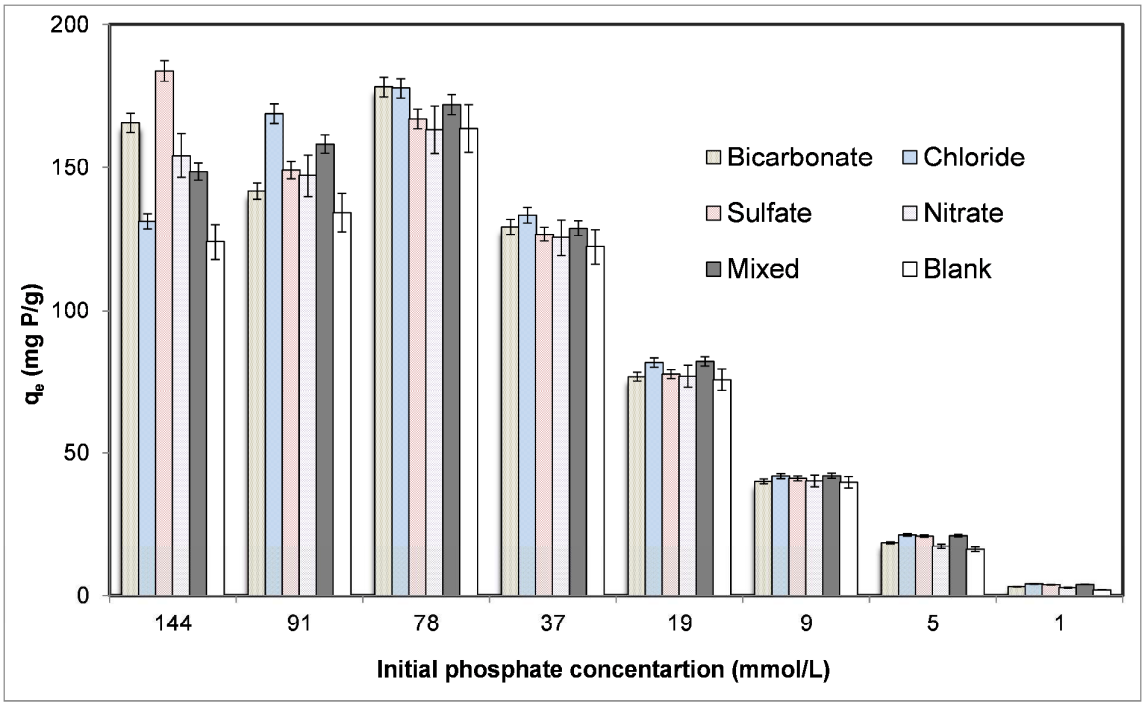
200
150
100
50
0
q_e (mg P/g)
Bicarbonate
Chloride
Sulfate
Nitrate
Mixed
Blank
144
91
78
37
19
9
5
1
Initial phosphate concentartion (mmol/L)

Fig. 8.

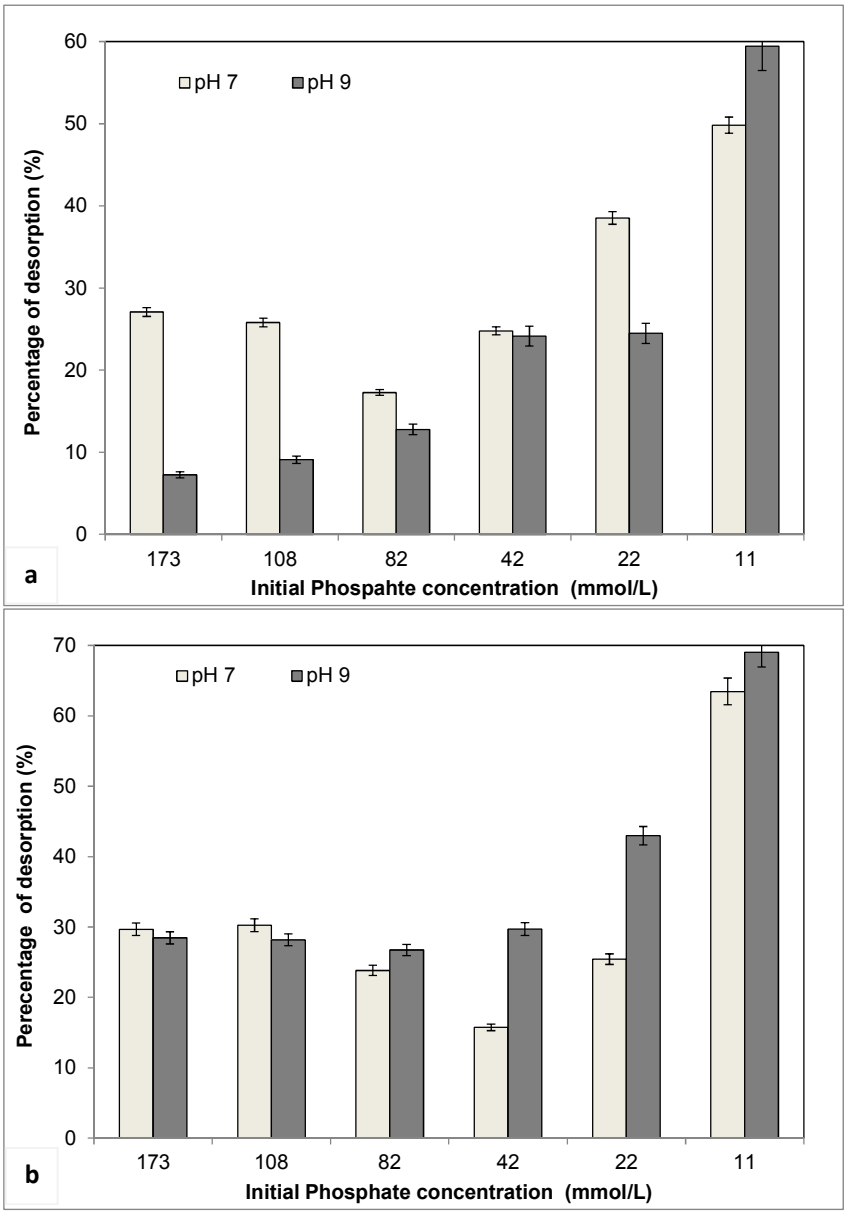
pH 7
pH 9
Percentage of desorption (%)
60
50
40
30
20
10
0
173
108
82
42
22
11
a
Initial Phospahte concentration (mmol/L)
pH 7
pH 9
Perecentage of desorption (%)
70
60
50
40
30
20
10
0
173
108
82
42
22
11
b
Initial Phosphate concentration (mmol/L)

Fig. 9.

Supplementary material

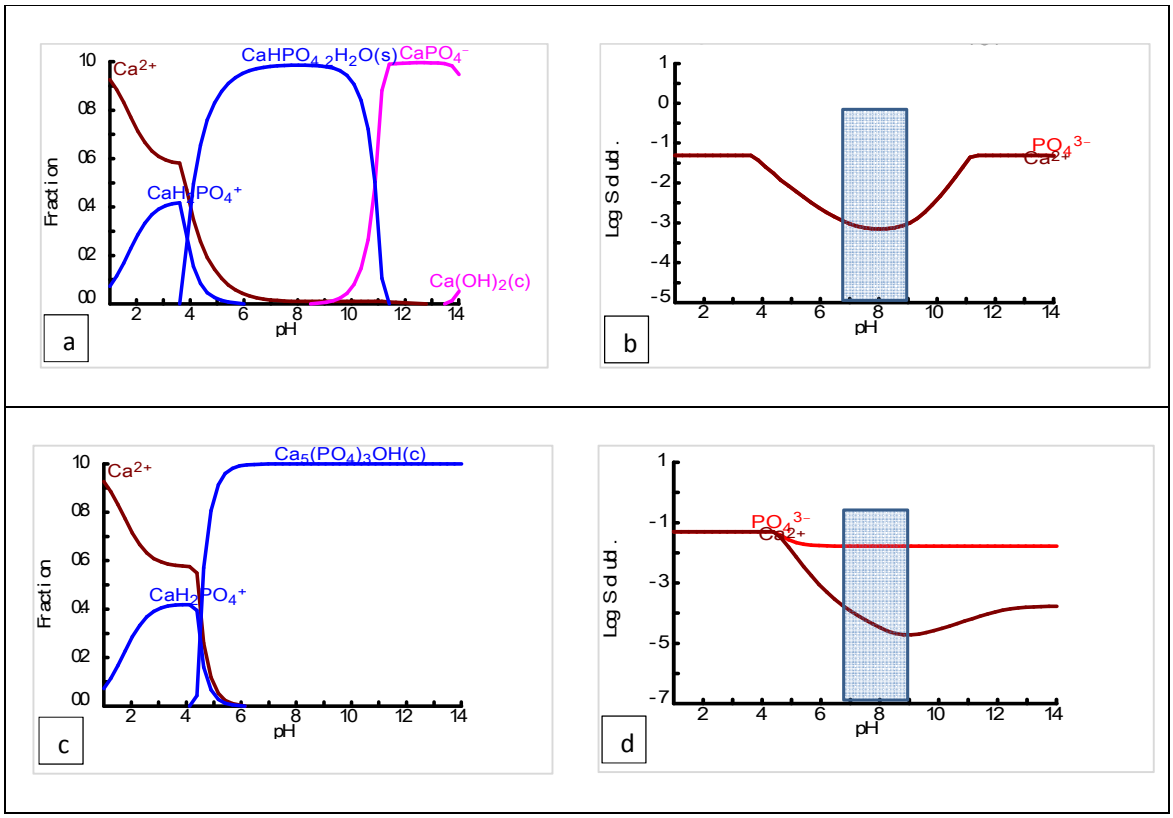

Fig. S1. Species distribution diagram and solubility as a function of pH for the system calcium and phosphate using the HYDRA-Medusa data base [55] for both phases: (a-b) $CaHPO_4.2H_2O$ (Brushite) and (c-d) $Ca_5(PO_4)_3OH$ (Hydroxyapatite). In the box is indicating the pH range evaluated (maximum and minimum values).